AD-A084 249 SCIENCE APPLICATIONS INC ANN ARBOR MI OPTICAL SCIENC--ETC F/G 20/6
INFRARED ELECTRO-OPTIC SYSTEM PERFORMANCE EFFECTS DUE TO ABSORP--ETC(U)
JAN 80 D H LESLIE, P G EITNER, J L MANNING DAEA18-73-A-0127
UNCLASSIFIED SAI-78-010-AA ERADCOM/ASL -CR-80-0127-2 NL

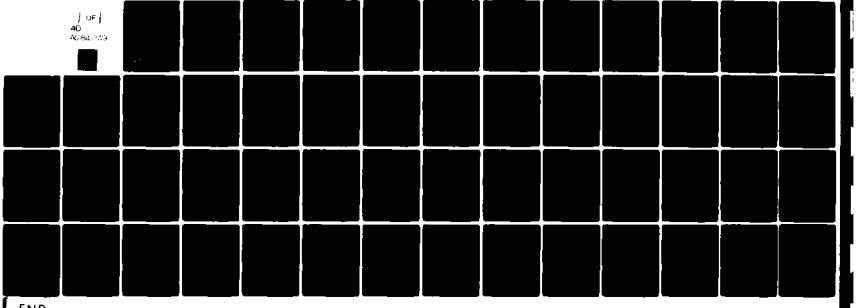

END
DATE FILMED
6-80
DTIC

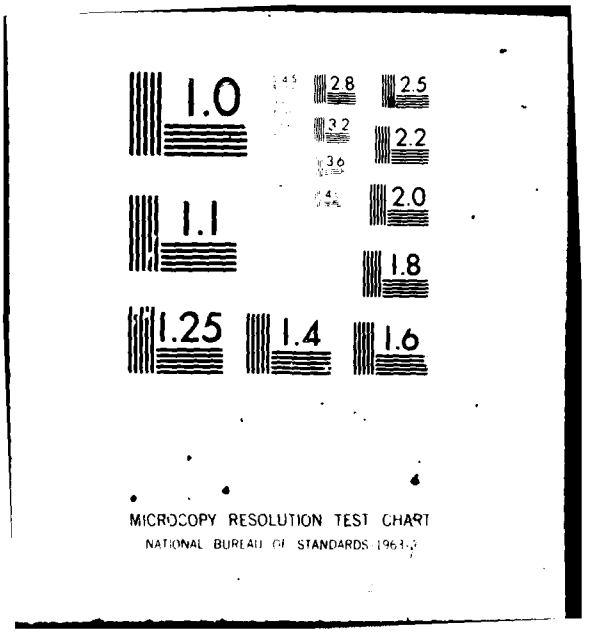
1.0
2.8
2.5
3.2
2.2
3.6
2.0
1.1
1.8
1.25
1.4
1.6
MICROCOPY RESOLUTION TEST CHART
NATIONAL BUREAU OF STANDARDS 1963-A

ASL-CR-80-0127-2

AD

Reports Control Symbol
OSD-1366

INFRARED ELECTRO-OPTIC SYSTEM PERFORMANCE EFFECTS DUE TO ABSORPTION BY BATTLEFIELD GASES

JANUARY 1980

Prepared by

D. H. Leslie
P. G. Eitner
J. L. Manning
S. M. Singer

Science Applications, Inc.
Optical Sciences Division
15 Research Dr.
Ann Arbor, MI 48103

Contract DAEA18-73-A-0127, BN05
SAI Project Number: 1-161-03-099-00

Contract Monitor: KENNETH O. WHITE

Approved for public release; distribution unlimited

US Army Electronics Research and Development Command
ATMOSPHERIC SCIENCES LABORATORY
White Sands Missile Range, NM 88002

NOTICES

Disclaimers

The findings in this report are not to be construed as an official Department of the Army position, unless so designated by other authorized documents.

The citation of trade names and names of manufacturers in this report is not to be construed as official Government indorsement or approval of commercial products or services referenced herein.

Disposition

Destroy this report when it is no longer needed. Do not return it to the originator.

Unclassified (18) ERADCOM/ASL

SECURITY CLASSIFICATION OF THIS PAGE (When Data Entered)

(19) **REPORT DOCUMENTATION PAGE**

READ INSTRUCTIONS BEFORE COMPLETING FORM

1. REPORT NUMBER: ASL-CR-80-0127-2	2. GOVT ACCESSION NO.: AD-A084 249
3. RECIPIENT'S CATALOG NUMBER:	
4. TITLE (and Subtitle): Infrared Electro-Optic System Performance Effects Due to Absorption by Battlefield Gases	5. TYPE OF REPORT & PERIOD COVERED: Technical Report
	6. PERFORMING ORG. REPORT NUMBER: SAI-78-010-AA (14)
7. AUTHOR(s): (10) D. H. Leslie, J. L. Manning, P. G. Eitner, S. M. Singer	8. CONTRACT OR GRANT NUMBER(s): (15) DAEA18-73-A-0127, BNO5
9. PERFORMING ORGANIZATION NAME AND ADDRESS: Science Applications, Inc., 15 Research Drive, Ann Arbor, Michigan 48103	10. PROGRAM ELEMENT, PROJECT, TASK AREA & WORK UNIT NUMBERS: 1-161-03-099-00
11. CONTROLLING OFFICE NAME AND ADDRESS: US Army Electronics Research and Development Command, Adelphi, MD 20783 (12) 54 (11)	12. REPORT DATE: Jan 80
	13. NUMBER OF PAGES: 50
14. MONITORING AGENCY NAME & ADDRESS (if different from Controlling Office): Atmospheric Sciences Laboratory, White Sands Missile Range, NM 88002	15. SECURITY CLASS. (of this report): Unclassified
	15a. DECLASSIFICATION/DOWNGRADING SCHEDULE:

16. DISTRIBUTION STATEMENT (of this Report)

Approved for public release; distribution unlimited

17. DISTRIBUTION STATEMENT (of the abstract entered in Block 20, if different from Report)

(9) Final rept.

18. SUPPLEMENTARY NOTES

Contract Monitor: Kenneth O. White

19. KEY WORDS (Continue on reverse side if necessary and identify by block number)

Battlefield Gas
Infrared Spectra
Laser Absorption

20. ABSTRACT (Continue on reverse side if necessary and identify by block number)

Estimates of laser and broadband infrared gaseous absorption are provided for several land battlefield scenarios. Quantity, dispersion, and concentration are discussed using a simple diffusion model. Sources treated are vapor products of TNT and RDX explosions, land fires, and vehicle emissions.

DD FORM 1 JAN 73 1473 EDITION OF 1 NOV 65 IS OBSOLETE

Unclassified

SECURITY CLASSIFICATION OF THIS PAGE (When Data Entered)

Foreword

The work for this report was done by D. H. Leslie, P. G. Eitner, J. L. Manning, and S. M. Singer of the Optical Sciences Division of Science Applications, Inc., at Ann Arbor, Michigan. The Principal Investigator for the Project was Dr. R. E. Meredith. The contracting officer technical representative was Dr. K. O. White, Atmospheric Sciences Laboratory, White Sands Missile Range, NM. The final report preparation was supervised by G. D. Currie.

CONTENTS

LIST OF ILLUSTRATIONS

LIST OF TABLES

1. INTRODUCTION

It is important to estimate the magnitude of infrared absorption by gases likely to be present in a land battle situation. Absorption regions of interest include those at emission lines of certain lasers, for example, the CO_2 laser which emits at 9 - 11 μm (especially P(20) at 10.59 μm), the DF laser which emits at several wavelengths around 3.8 μm, and the Nd-Yag laser at 1.06 μm. The need for estimates of absorption is clear. It is essential to know in advance whether the operation of systems such as FLIR and TOW anti-tank weapons, for example, are adversely affected by infrared absorption from gases produced by battlefield activity.

Our task is to evaluate the effects of gases in the battlefield on atmospheric transmission at the frequencies where laser and broadband devices commonly operate. We first estimate amounts of gaseous products due to explosion of munitions. Combustion products are examined and estimates of vehicle emission are given. With estimates of the quantity of various gases likely present, a point source dispersion model is used to estimate volume concentrations. Published IR absorption coefficients are then used to estimate absorption for reasonable concentrations over a 1 kilometer path of uniformly mixed and dispersed battlefield gas.

2. SOURCES

By treating several specific and likely scenarios of a hypothetical land encounter we can provide estimates of the concentrations of important infrared active gases. We first treat gaseous products of explosive detonations (non-nuclear) such as would accompany a modern land encounter. Then the possiblility of chemical interactions resulting from the detonation in air is examined for likely concentrations of species such as ozone. Chemical propellants emanating from artillery emplacements further add gas to the area and are examined. Products due to combustion of foliage and other materials which may be present in the battlefield are also treated.

2.1 PRODUCTS OF MUNITION EXPLOSIVES

A munition explosion causes a shock wave which defines the boundary of chemical activity. The rapid combustion of the solid payload of an artillery shell, for example, yields gaseous and aerosol products which can react with each other and with the atmosphere. In this study we are concerned primarily with the final gasous products.

Most artillery payloads, both NATO and foreign, contain one of the explosives listed in Table 1 [1]. Other common

TABLE 1. COMMON EXPLOSIVES

Explosive Name	Chemical Formula	Packing Density
TNT trinitrotoluene	$C_7H_5N_3O_6$	1.6 g/cm^3
RDX cyclotrimethylene trinitramine	$C_3H_6N_6O_6$	1.8 g/cm^3
HMX cyclotetramethylene tetranitramine	$C_4H_8N_8O_8$	1.9 g/cm^3

military explosives are "composition B" which is composed of a 60-40 mix of RDX and TNT with a 1% wax binder, and Octol, a mix of TNT and HMX [2]. An explosive common among non-NATO nations is "Amatol" consisting of ammonium nitrate (NH_4NO_3) and TNT. Given that the great majority of heavy artillery payloads belong to the CHNO family, we expect gaseous products of combustion to consist of molecules having C,H,N,O constituents.

Although the great majority of explosives in common use belong to the CHNO family, some other explosives contain more infrared interesting constituents. Some of these explosive families are:

Fluoronitirobenzenes: CNOF, CHNOF systems
such as FEFO: $C_5H_6N_4O_{10}F_2$

Liquids: CNF, CHNF systems

Be/Br F_5 system

Zero Hydrogen systems

The list of chemical products of detonation is quite extensive since these systems include halogen atoms which are very reactive. Appendix 1 is a list of compounds which may appear as detonation products. The number of compounds listed in Appendix 1 which contain halogen atoms indicates the degree of complexity which is added to the chemistry by the presence of halogens in the explosive. Significant use of these explosives is not expected [1, 2], and we shall restrict our analysis to the CHNO family of explosives.

In order to assess probable types and quantities of gaseous products, we applied the TIGER computer code [3] to TNT and RDX for the most common packing densities. TIGER calculations combine the chemistry and the thermodynamics of the explosion. The code produces shock velocities and thermodynamic variables at various points along an isentrope from the detonation point.

Concentrations of gaseous and solid products are given with the thermodynamic variables. The system expands from detonation at the Chapman-Jougnet (C-J) point at roughly 10^5 atmospheres pressure. (The C-J point is operationally defined as that point on the PV plane where decomposition of the solid into its products is complete.) Figures 1 and 2 show how the constituents vary as the systems expand at constant entropy from the C-J point to atmospheric pressure. The number of moles of each constituent per kilogram of original explosive is also plotted as a function of total pressure on each figure. The greatest difference between TNT and RDX is the amount of solid carbon (assumed graphite form) remaining. This is not surprising since TNT is C_7... and RDX is C_3... .

Tables 2, 3, and 4 list the detonation products from TNT, RDX and other explosives, respectively. TIGER results are listed along with results of other calculations and observations from the literature. In Section 4 the infrared properties of these gases will be examined.

The chemistry model in the TIGER code is a chemical equilibrium model. Chemical equilibrium is, effectively, the assumption that the chemistry proceeds on a much faster time scale then the expansion process; that is, the concentrations at any given time during the expansion are the same as would be found by stopping the expansion at that time and allowing the chemistry to proceed until the concentrations reach steady state values. The chemical equilibrium assumption is valid at high temperatures and pressures. Later in the expansion, however, the chemical equilibrium assumption is less accurate because some of the reaction rates decrease as the cloud expands and cools. Because of this, the final composition of the cloud at ambient pressure and temperature is best represented by chemical equilibrium concentrations at some higher pressure or temperature. "Equilibrium freeze-out" temperatures of 1600° to 1900°K are often

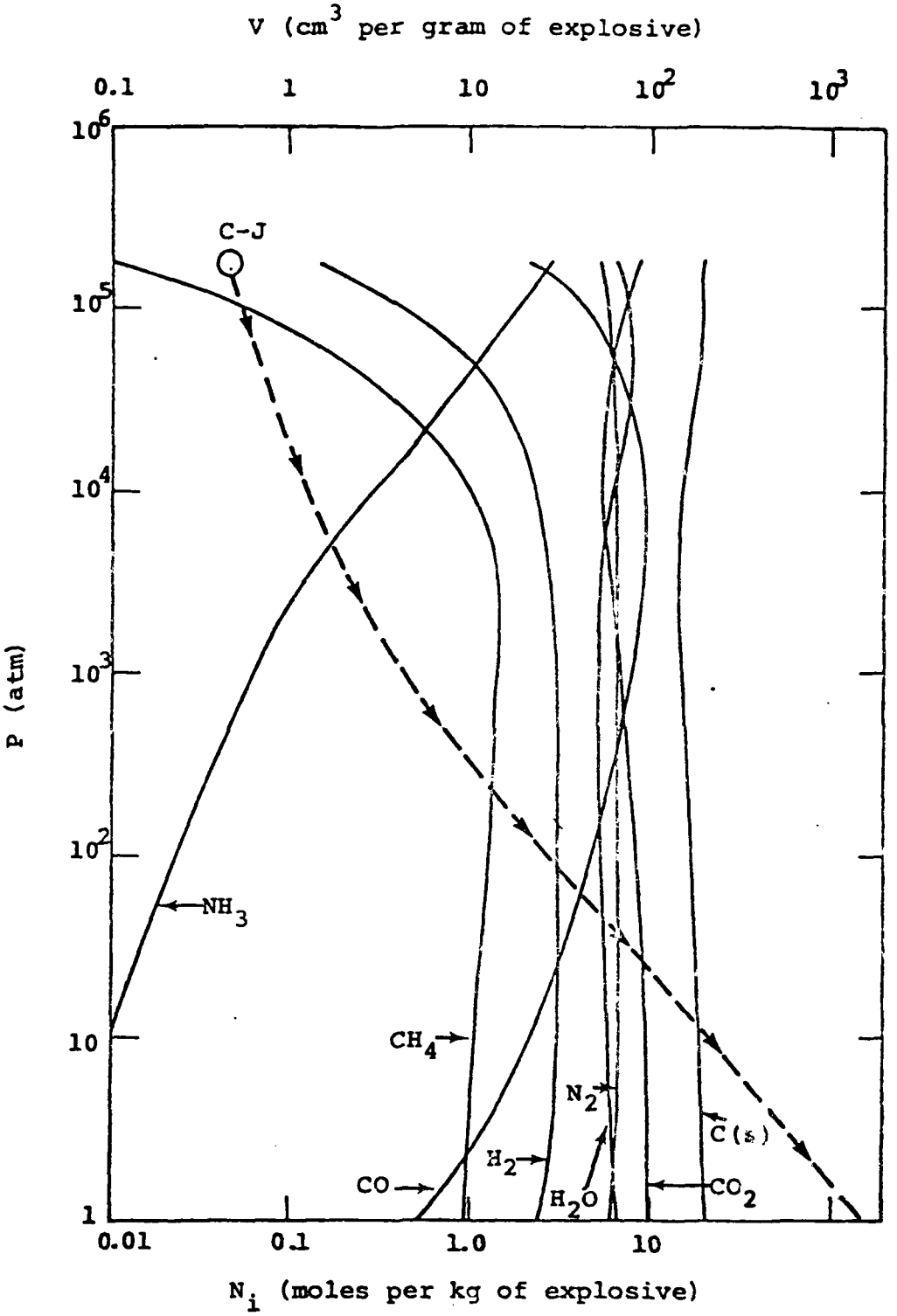

FIGURE 1. CALCULATED PRODUCTS FROM TNT EXPLOSION AND P-V CURVE OF SHOCK WAVE (DASHED CURVE)

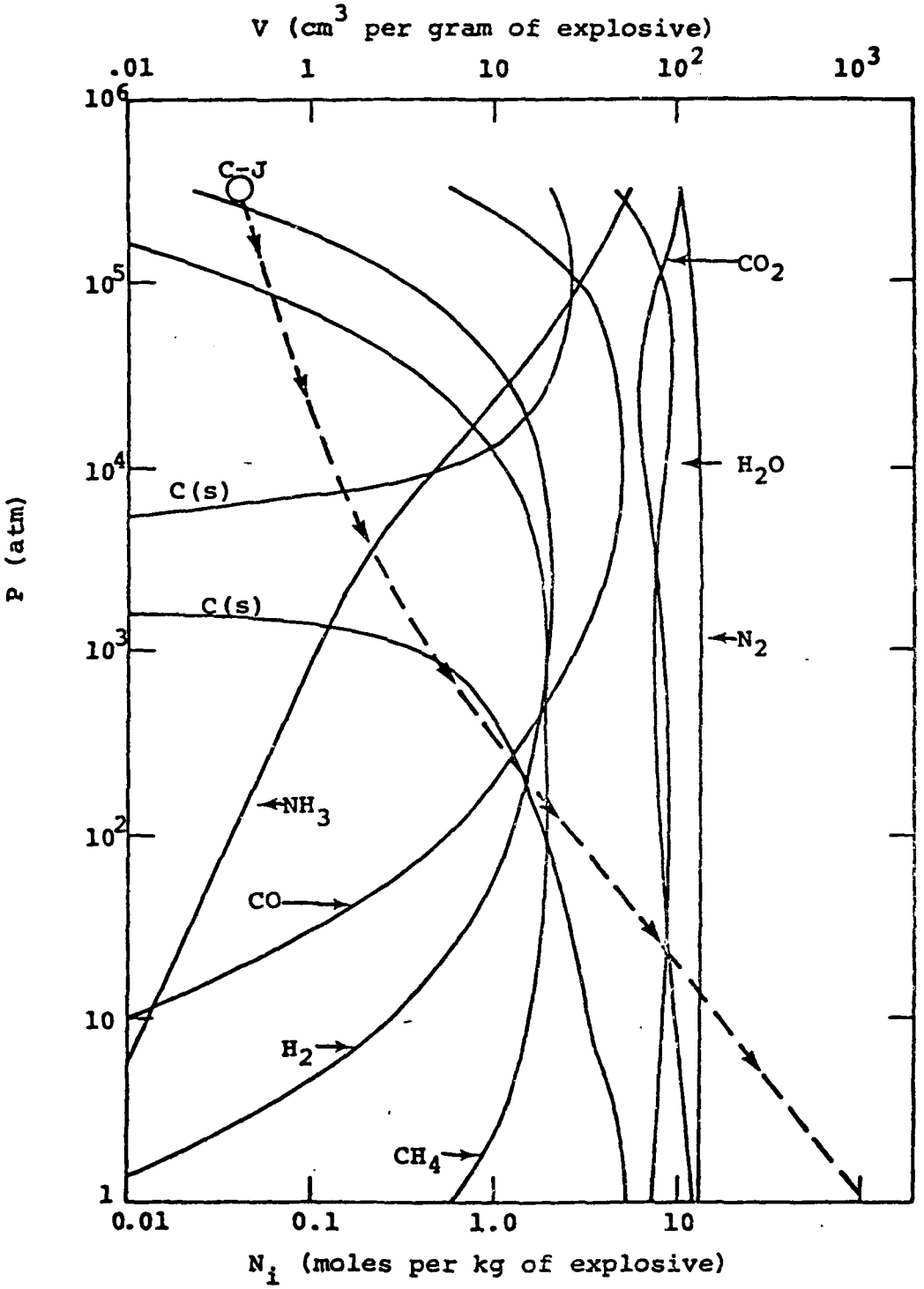

FIGURE 2. CALCULATED PRODUCTS FROM RDX EXPLOSION AND P-V CURVE OF SHOCK WAVE (DASHED CURVE).

TABLE 2. DETONATION PRODUCTS FROM TNT
(MOLES PER KILOGRAM OF EXPLOSIVE)

PRODUCT	TIGER[a]	TIGER[b]	OBSERVED[c]	OBSERVED[d]
CO_2	8.4	5.5	5.5	5.5
N_2	6.5	6.5	---	5.8
CO	6.0	9.4	9.4	8.7
H_2O	5.1	6.0	6.1	7.1
H_2	3.1	2.4	1.6	2.0
CH_4	1.7	1.1	0.4	0.4
NH_3	0.04	0.2	1.5	0.7
C(S)	15.7	14.8	14.6	16.1
HCN	10^{-5}	---	---	0.1
C_2H_6	---	---	---	0.02

a) $10^2 - 10^3$ atmospheres, packing density ρ=1.6 gm/cm^3, JCZ3 equation of state. (See Reference 3.)

b) 1800°K "freeze-out" temperature, ρ = 1.6 gm/cm^3, JCZ3 equation of state.

c) Haid and Schmidt, as reported by Cook [7]. ρ = 1.59 gm/cm^3.

d) Ornellas [6], ρ = 1.53 gm/cm^3.

TABLE 3. DETONATION PRODUCTS FROM RDX
(MOLES PER KILOGRAM OF EXPLOSIVE)

PRODUCT	TIGER[a]	TIGER[b]	COOK[c]	RUBY[d]
CO_2	8.8	6.4	6.8	6.7
N_2	13.0	13.1	12.8	13.4
CO	1.4	5.0	3.0	0.7
H_2O	7.8	9.1	5.6	13.0
H_2	1.7	1.6	0.2	---
CH_4	2.0	0.8	---	0.1
NH_3	0.06	0.8	1.1	0.2
C(S)	1.0	1.3	---	6.1
CH_3OH	---	---	2.4	---

a) $10^2 - 10^3$ atmospheres, packing density ρ = 1.8 gm/cm^3, JCZ3 equation of state [1,3].

b) 1800°K "freeze-out" temperature, ρ = 1.8 gm/cm^3, JCZ3 equation of state.

c) calculated values, ρ = 1.6 gm/cm^3, reference 7.

d) BKW equation of state, reference 8.

TABLE 4. DETONATION PRODUCTS FROM AMATOL, HMX, AND FEFO (MOLES PER KILOGRAM OF EXPLOSIVE)

PRODUCT	AMATOL 80/20[a]	HMX OBSERVED[b]	FEFO OBSERVED[c]
CO_2	6.1	6.5	9.9
N_2	11.2	12.4	6.3
CO	0.1	3.6	5.9
H_2O	22.0	10.7	6.7
H_2	0.06	1.0	0.14
CH_4	---	0.13	0.003
NH_3	---	1.3	0.07
C(S)	---	3.3	0.0
HCN	---	0.03	---
C_2H_6	---	0.003	---
HF	---	---	5.8
CF_4	---	---	0.0

a)80% NH_4NO_3, 20% TNT, calculated values, packing density ρ = 1.0 gm/cm^3, reference 7.

b)ρ = 1.89 gm/cm^3, reference 4.

c)ρ = 1.60 gm/cm^3, reference 1.

used [1,4]. Other sources [5] suggest using TIGER results at a point in the expansion where the pressure is between 100 and 1000 atmospheres.

In Tables 2 and 3 we list TIGER results using both methods. The results are similar with two notable exceptions: the CO concentrations are somewhat higher using a "freeze-out" temperature, and the predicted NH_3 concentation is roughly an order of magnitude larger with the "freeze-out" temperature method than it is with the pressure method. There is no consensus as to which of these methods is more reliable, and we do not presume to be able to draw any such conclusion. We can only note that our results contain some uncertainty in the CO and NH_3 concentrations.

Table 2 contains results of observations of detonation products made by Ornellas [6] using a detonation calorimeter. Although only fair agreement with predictions is obtained, Ornellas did not report observation of significant quantities of constituents not listed in Table 2. The measurements were confined to the calorimeter volume and may differ from what is expected for an unconfined volume as found in the battlefield scenario. Calculations by Cook [7] indicate methyl alcohol as a product of RDX combustion. We have been unable to substantiate Cook's results. No observation of CH_3OH has been found, and the program active libraries of RUBY and TIGER do not list CH_3OH, indicating that the authors of these codes do not consider methyl alcohol as a possible detonation product [8].

A similar situation is found for HCN. Cook reports HCN as a product of TNT combustion, but our own calculations using TIGER yielded 10^{-5} moles per kilogram, which is quite negligible. Although Cook's excellent book is considered a reference work in many respects, significant advances in both computational techniques and equations of state have occurred since its publication (1958). This may account for the difference.

Another possible gas source we investigated is the production of propellant combustion gases from artillery batteries, rocket launchers, etc. According to H.M. Sheinfield most propellants belong to the CHNO family and the gas products are similar to those of the CHNO explosives [9]. Although clouds of smoke frequently linger near munition launchers, the amount of gas produced is not sufficient to generate significant optical depths of infrared active gases.

2.2 AIR CHEMISTRY FROM DETONATIONS

When a conventional explosive detonates, a shock wave is generated. The temperature and pressure conditions within this air blast are sufficient to induce the formation of relatively large quantities of infrared active species including O_3 and NO_x. Preliminary calculations have bounded the quantity and longevity of these species [10].

Detonation effects have been simulated with a well-tested one-dimensional blast wave version of the HELVA hydrodynamics code. In this application the explosion is described by a self-similar solution of a detonation wave propagating within the high explosive material. Calculations employ an equation of state with pressure proportional to the square of the density. The evolution of the system is traced by finite difference integration of the conservation equations. The air blast described in this manner produces the environment which drives the formation of O_3 and NO_x.

A simple model for air chemistry occurring in the blast wave is used to place an upper bound on the amounts of O_3 and NO_x formed. The formation of nitrogen oxides has been modeled by the modified Zel'dovich mechanism, appropriate for somewhat less severe conditions. The formation of ozone is modeled simply by the dominant three-body recombination reaction. Table 5 shows that sizable amounts of both O_3 and NO_x are predicted for even the smallest blasts of interest for battlefield applications.

After creation of these species by the detonation and initial blast chemistry, a simple smog photochemistry model (see Appendix 2) is used to examine the resultant evolution of the species. It is noted [10] that the quasi-steady state distribution is very sensitive to the initial ratio of O_3 to NO_x, and to the presence of hydrocarbons from other sources. As pointed out in the previous section, TNT produces considerably more solid carbon than RDX. This difference should also result in different O_3 and NO_x equilibrium concentrations for TNT (high carbon content) and RDX (low carbon content) shock generated air chemistry. In the units of Table 5 we expect approximately 2 moles O_3 and 0.3 moles NO per kilogram tetryl at three milliseconds after the blast. Although the above amounts are significant with regard to infrared transmission, they decrease by orders of magnitude in 0.1 to 1.0 seconds. The most important means for dissipation of O_3 and NO is:

$$O_3 + NO \rightarrow NO_2 + O_2$$

TABLE 5. O_3 AND NO_x AT 3 MILLISECONDS AFTER BLAST

Mass Tetryl*	Moles O_3	Moles NO_x
4 Kg	8.6	1.2
10 Kg	24.3	2.5

*Tetryl is a common explosive belonging to the CHNO family ($C_7H_5O_8N_5$). It is often used as an intermediate charge to ignite a main charge of explosive, such as TNT, although it may itself be used as a main charge. The results presented here are expected to be order-of-magnitude representative for CHNO explosives.

Hence, the active and infrared interesting species O_3 and NO tend to rapidly combine to yield the relatively chemically inert species diatomic oxygen and nitrogen dioxide. The remainder depends critically on the initial concentration of O_3 and NO. The presence of large amounts of hot particulate carbon may influence the late term chemistry. At any rate, the steady state quantities estimated by the air chemistry model are not sufficient to warrant further consideration here, although the transient amounts may be important for some E-O systems. The greatest uncertainty in these calculations is the role of the hot particulate carbon - O_3 and - NO_x chemistry and its proclivity for forming C-H bonds. This question may deserve experimental examination since O_3 absorbs strongly both at 10 μm and in the long wavelength submillimeter region.

2.3 GASES FROM LIKELY COMBUSTIBLES

Certainly combustion of areas surrounding a battlefield scene will produce gaseous products. The products produced depend critically on the nature of the surroundings. Table 6 lists the absorption coefficients in the 10 μm region for products of burning hay, rubber, and gasoline. The units are $cm^{-1}/g/l$ which is interpreted as fractional absorption per cm path per (gram/liter) where (gram/liter) is the initial mass of the fuel divided by the volume of the gas cell at one atmosphere pressure. The data is thus conveniently scaled. Figures 3 to 5 are reproductions from reference 11. Section 4 will treat the magnitude of absorption expected once the dispersion, which will be discussed in Section 3, is included.

TABLE 6. ABSORPTION BY FIRE PRODUCTS AT 10 μm

Burning Dry Hay:	CH_3OH	.04	cm^{-1}/gram/liter
	C_2H_2	.01	
Burning Rubber:	C_2H_4	.15	
	C_4H_6	.15	
Burning Gasoline:	C_2H_4	.03	

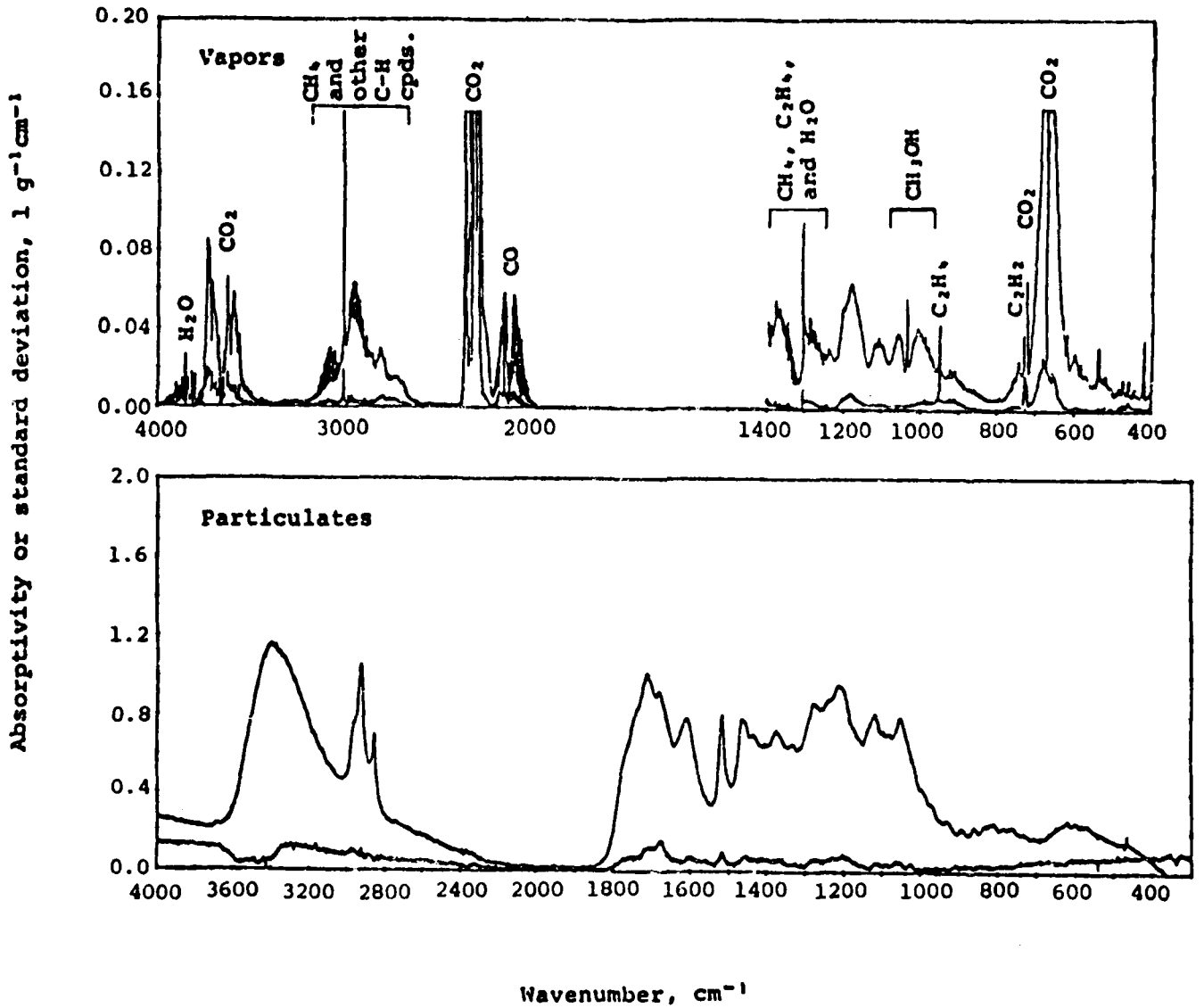

FIGURE 3. SPECTRA OF COMPONENTS OF SMOKE FROM BURNING DRY HAY

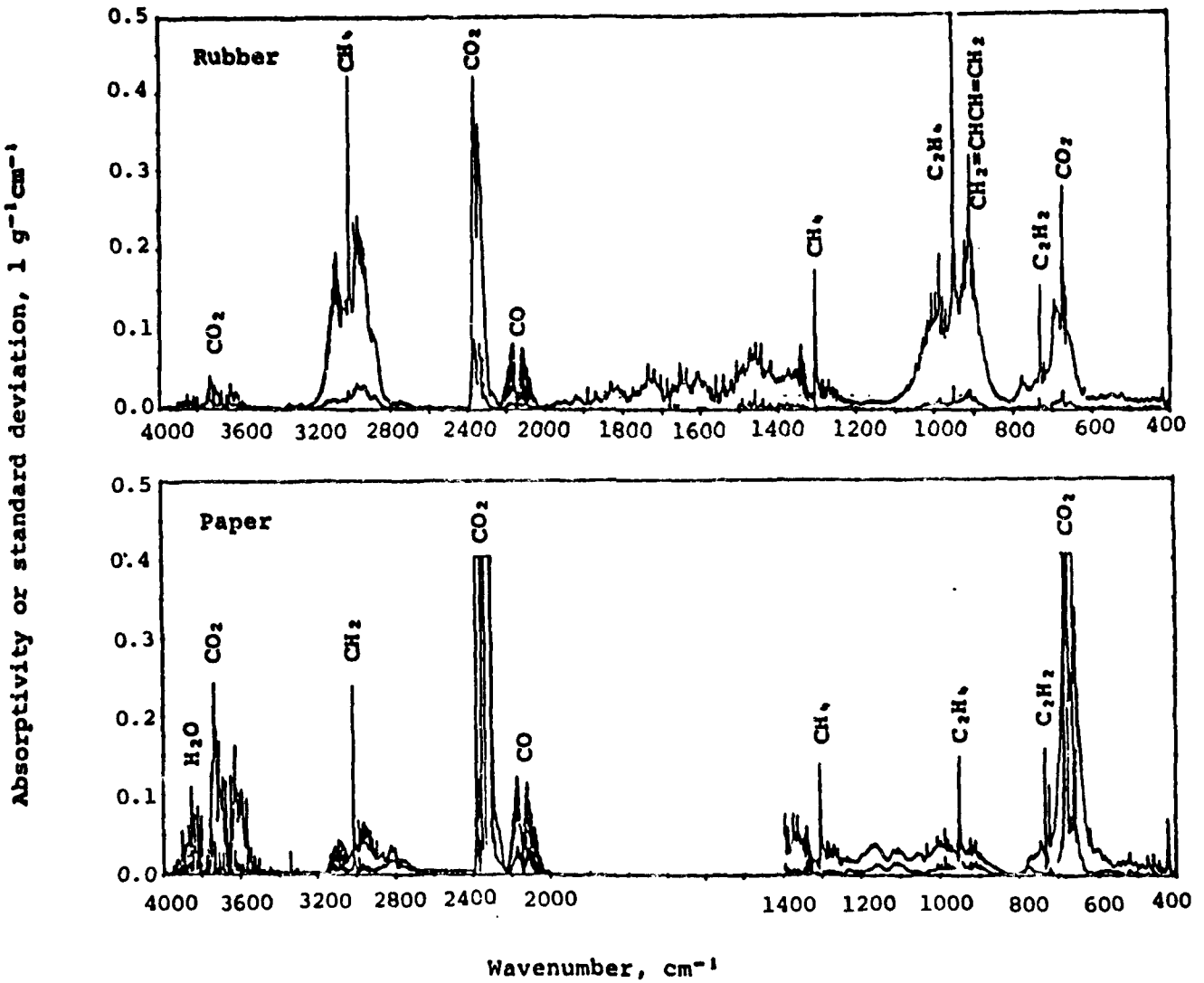

FIGURE 4. SPECTRA OF VAPORS FROM BURNING RUBBER AND PAPER

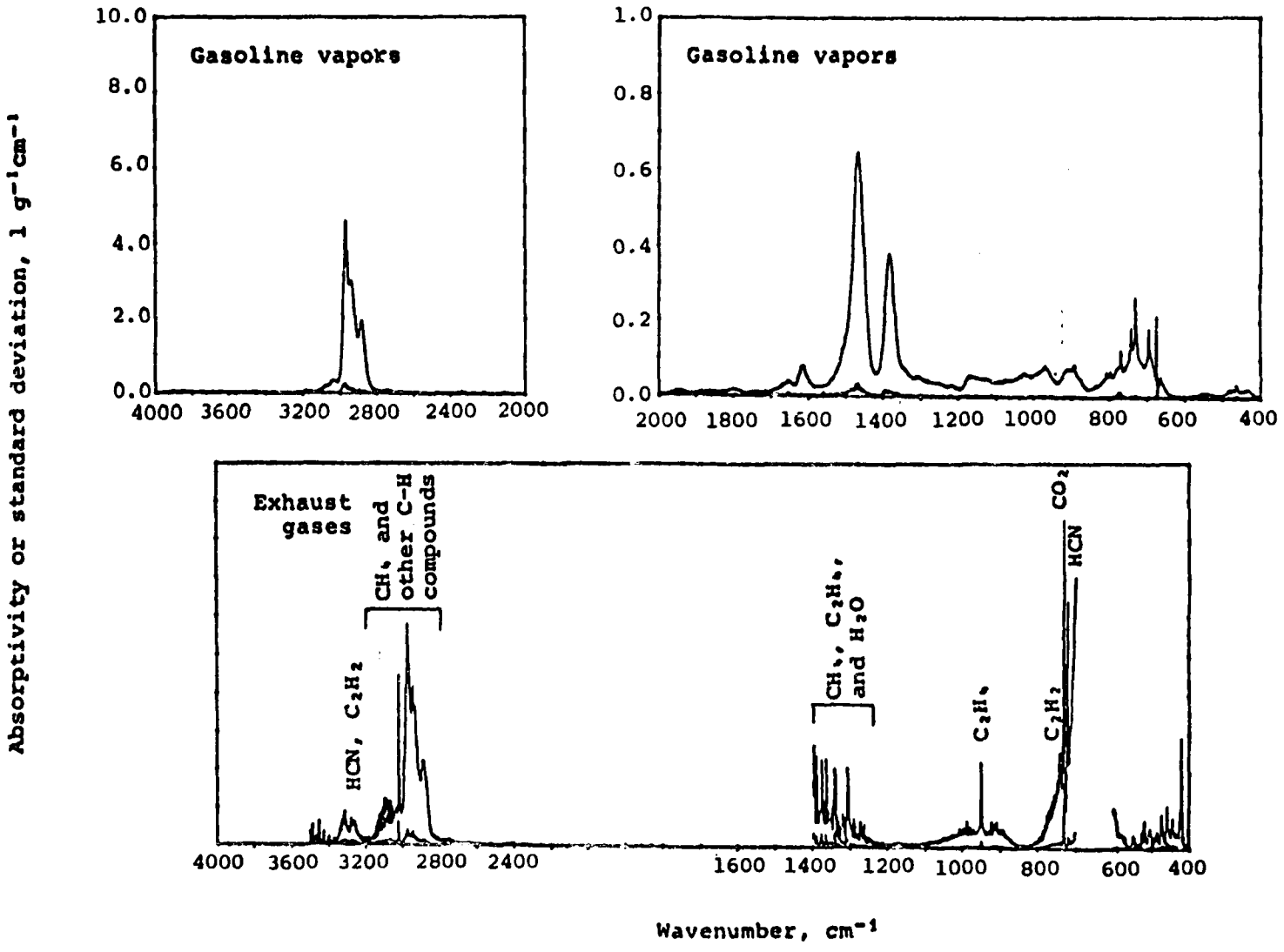

FIGURE 5. SPECTRA OF GASOLINE VAPORS AND EXHAUST GASES

2.4 VEHICLE EMISSIONS

Since vehicle fuels are primarily hydrocarbons, combustion yields no rare molecules. The most interesting product from the infrared standpoint is ethylene since one of its absorption bands lies in the 10 μm window. From the Caterpillar Tractor Company [12] we have learned that the concentration of ethylene in the exhaust of a 210 HP, 636 cubic inch direct injection diesel engine (with no catalytic converter) is 30 parts per million. We wish to estimate the amount of ethylene produced by one tank engine. We can estimate the rate of emission of ethylene by making a rough estimate of the rate of exhaust emission from the displacement and multiplying by 30×10^{-6}. In doing this calculation we note that two factors must be included. First, for a four cycle engine, only half the cylinders fire during one engine revolution, introducing a factor of 1/2. Second, the displacement provides gas volume at the intake manifold pressure, and this must be adjusted to atmospheric pressure by multiplying by the ratio of manifold pressure to atmospheric pressure. Assuming an engine twice the above size running at 1000 rpm with 0.8 atmospheres manifold pressure, we have

$$\left(\frac{1270\ \text{in}^3}{2\ \text{rev}}\right) \times \left(\frac{1000\ \text{rev}}{\text{min}}\right) \times \left(\frac{0.8\ \text{atm}}{1.0\ \text{atm}}\right)$$

$$\times \left(\frac{2.54\ \text{cm}}{\text{in}}\right)^3 \times \left(\frac{1\ \ell}{10^3\ \text{cm}^3}\right)$$

$$\times \left(30 \times 10^{-6}\right)$$

$$= 0.25\ \frac{\text{liters}}{\text{min}}\ \text{of}\ C_2H_4$$

Other gaseous combustion products from the large diesel engines which power tanks are CO, NO, aldehydes, and relatively large quantities of CO_2 and H_2O. The CO_2 and H_2O emission can be estimated by considering stoichiometric burning of diesel fuel [13]:

$$2\ CH_{1.8} + 2.9\ O_2 + 10.93\ N_2 \rightarrow 2\ CO_2 + 1.8\ H_2O + 10.93\ N_2$$

The exhaust consists of 2 moles of CO_2 and 1.8 moles of H_2O in 14.7 moles of exhaust, or 13.6% CO_2 and 12.2% H_2O by volume. This "reaction" is really a composite of a set of reactions, one for each of the various fuel molecules. In addition there is a rather extensive set of reactions involving impurities in the fuel and in the air and phenomena such as incomplete combustion to produce a variety of "pollutant" gases and aerosols.

Typical emission rates for CO, NO, and aldehydes are 6, 8 and 0.3 grams per horsepower per hour, respectively [14,15]. Table 7 shows emissions in liters per minute which result from analyses similar to that given above for ethylene.

TABLE 7. VEHICLE EMISSIONS: EXHAUST GASES FROM A LARGE DIESEL ENGINE, IN LITERS PER MINUTE (STP).

CO_2	1130
H_2O	1020
CO	40
NO	50
Aldehydes	2
Ethylene	0.25

3. DISPERSION MODEL

Of necessary importance to the problem of gases affecting E-O systems is the amount of gas in the beam path. As the cases considered here are primarily point sources, we need to know how the gas will disperse when released. For short times we consider a "short time model" of a 10m x 10m x 10m cube in which a quantity of gas, say 1 mole, is uniformly mixed at atmospheric pressure. For 1 mole (22.4 liters at STP) the concentration is 22.4 parts per million in the cube of 10^6 liter volume, and the path through the cube is taken to be 10 meters. We can then, in Section 4, make estimates of absorption in the convenient units of (km^{-1}/ppm).

For a more reasonable estimate of dispersion applicable for longer times we have done a series of calculations for point sources using the diffusion equation $\partial c/\partial t = k\nabla^2 c$ (where c is the concentration, mass per unit volume, of the diffusing gas) for a reasonable range of turbulent diffusion constant k, assumed isotropic. Advection by wind is treated separately. Using appropriate boundary conditions for a spherically symmetric solution (we ignore the half plane aspects of a ground blast) and conserving total mass Q we arrive at [16]

$$c(x,y,z,t) = \frac{Q}{8(\pi kt)^{3/2}} \exp\left(-\frac{x^2+y^2+z^2}{4kt}\right)$$

With z vertical and x downstream we can account for buoyancy and wind advection via the transformations

$x \rightarrow x - \bar{u}t$ $\quad \bar{u}$ = mean wind speed

$z \rightarrow z - h(t)$ $\quad h(t)$ = height of centroid at time t

The buoyancy model is patterned after that suggested by Dumbauld [17, 18]:

$$h(t) = h_o + \left\{ \frac{3H}{C_p \pi \rho \alpha^3 s} \left[1 - \cos \sqrt{\frac{gs}{T}}\, t \right] \right\}^{1/4}$$

where h_o = initial source height
g = gravitational constant, 9.8 m/sec^2
H = total heat released by the explosion
C_p = specific heat at constant pressure
ρ = air density
T = air temperature
α = entrainment coefficient ($\sim$0.6)
s = $d\theta/dz$ = stability parameter
θ = potential temperature

The above expression is valid only until final time $t_f = \pi(gs/T)^{-1/2}$ after which the centroid is assumed stable at its final height $h(t_f)$.

The dispersion results are displayed in Figures 6 and 7. $R_{.5}$ and $R_{.9}$ are the radii containing 50% and 90% respectively of the total mass of gas released at a point source. From the buoyancy calculations we see that the centroid of the gas cloud rapidly rises to at least 30 meters, assuming a 1 kilogram explosion with 10^6 calories yield. The height scales as $H^{1/4}$ where H = yield, so 30 meters is a reasonable lower limit. Certainly late time cooling and mixing will alter the buoyancy result. But from our diffusion model a sphere of 30 meter radius also represents the minimum diffusion case for $R_{.9}$ at 30 minutes. Hence the late time distribution is taken to be confined to a sphere of radius 30 meters with its center 30 meters

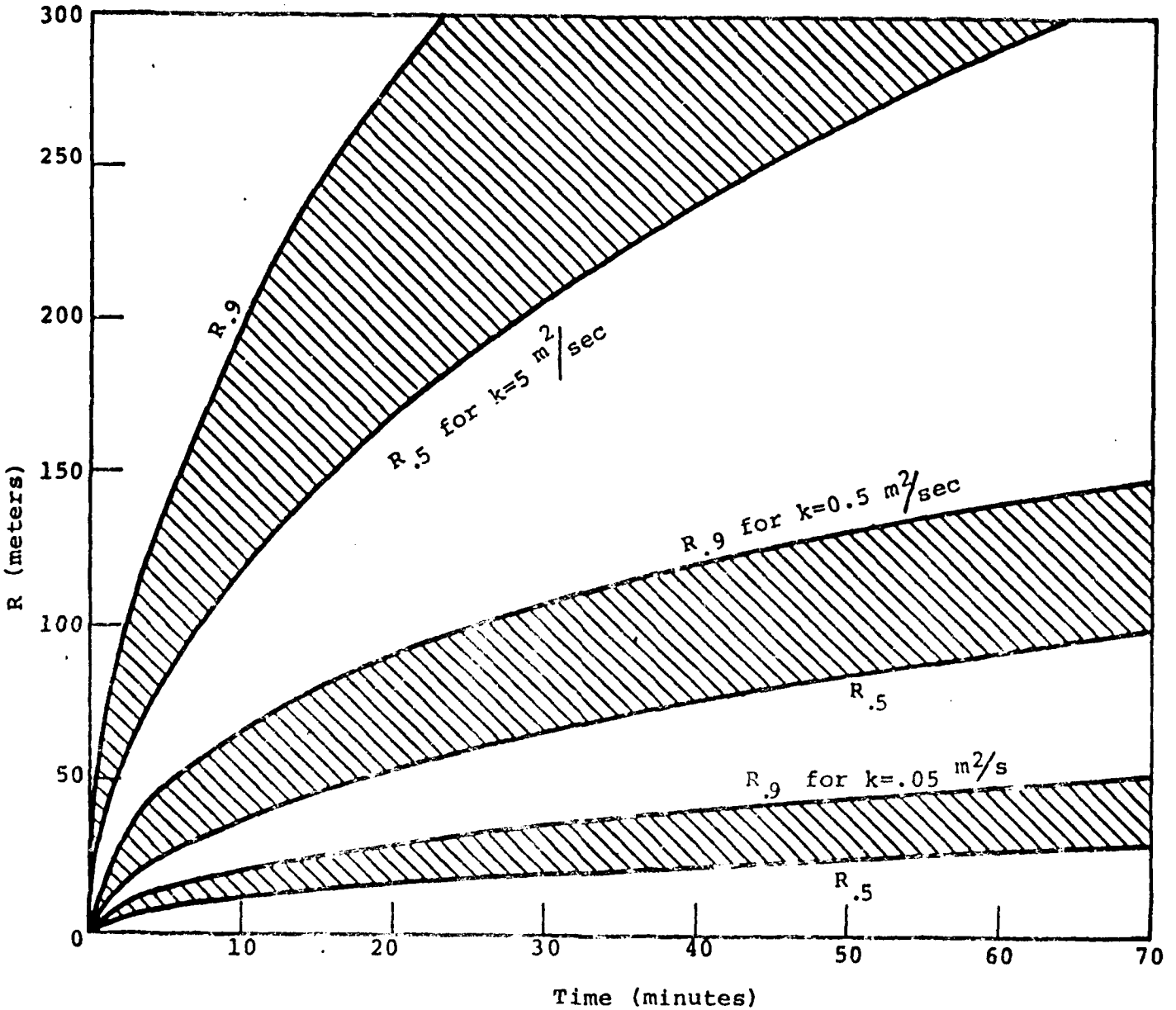

FIGURE 6. HALF-MASS RADIUS AND 90%-MASS RADIUS PREDICTED BY THE DISPERSION MODEL, FOR THREE DIFFUSION COEFFICIENTS

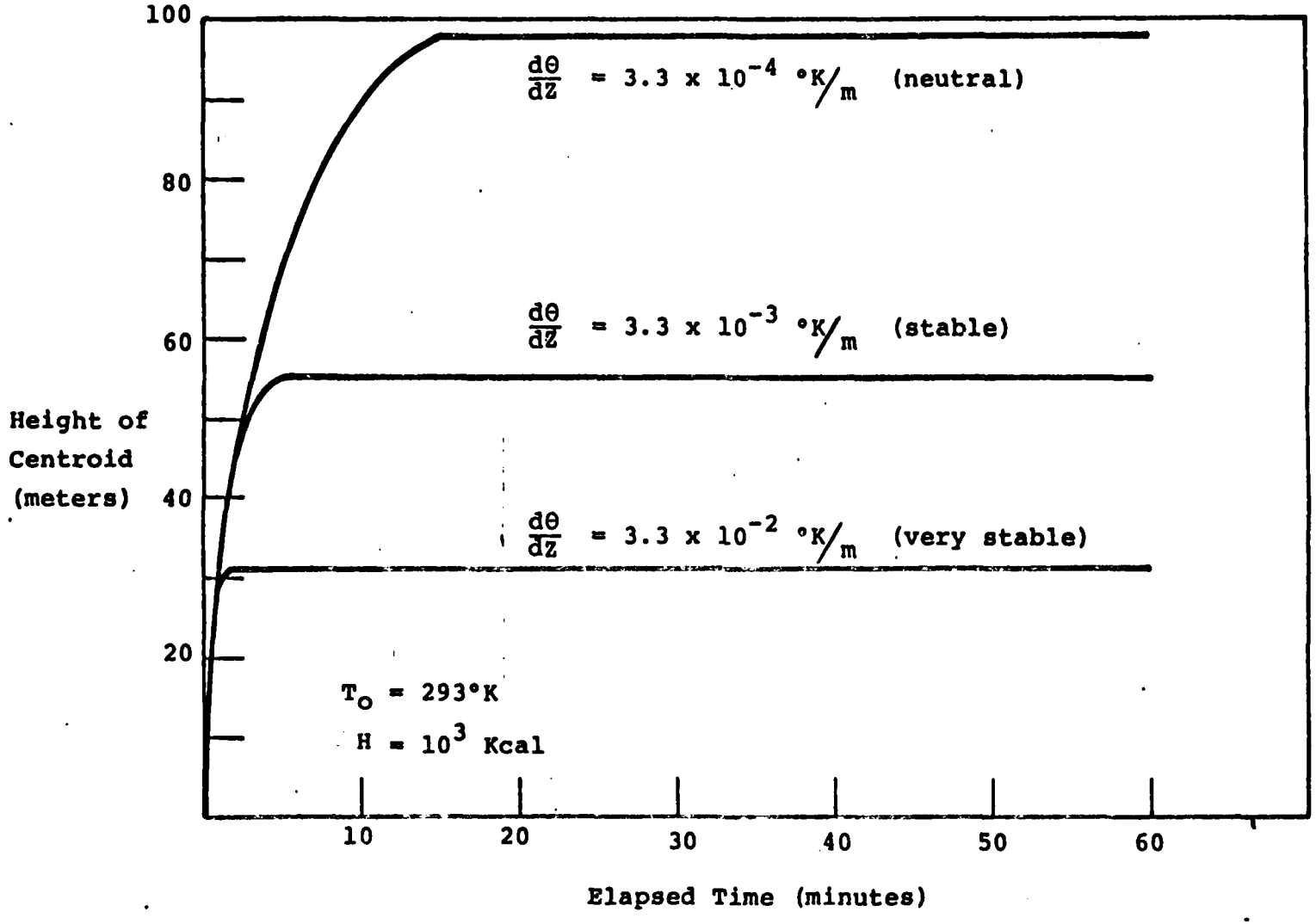

FIGURE 7. BUOYANCY MODEL FOR THREE TYPICAL VERTICAL GRADIENTS OF POTENTIAL TEMPERATURE

above ground. With neutral rather than very stable temperature gradients and turbulent rather than slow diffusion the volume appropriate could be 10 to 50 times larger with the same decrease in concentration and hence optical depth.

4. INFRARED ABSORPTION

In the previous sections we have considered likely sources of gas generated in the battlefield, and we have estimated quantities and extent of significant concentrations. In this section we will consider absorption strengths of gases which have absorption bands in the 8 - 12 μm, 3 - 5 μm and 1.06 μm IR regions.

4.1 EXPLOSION VAPORS

Since by quantity most of the products of munition explosions are also found in the ambient atmosphere it is instructive to evaluate a "worst case" estimate of gas concentrations following a sustained half hour artillery barrage. A reasonable averaging method is provided by assuming one "hit" per 10m x 10m area per 30 minutes for a total area of 1 km x 1 km [19]. We then take 60 meters as a ceiling for the case of maximum containment, since 60 meters is 30 meter buoyancy height plus 30 meter $R_{.9}$ radius. For 10^4 explosions of average payload 4 kilograms we have 4×10^4 kilograms of either TNT or RDX. The total volume is 6×10^{10} liters. Since the $R_{.9}$ radii overlap considerably for each 10m x 10m burst, we can assume a uniform mix. An E-O sensor then tries to see through one kilometer of path of uniformly mixed gas. The gas concentrations for this scenario are listed in Table 8 along with the atmospheric background concentrations for comparison.

It is clear from Table 8 that only CO is produced in quantities significant compared to ambient concentrations, 300 to 1000 times ambient. The CO fundamental is at 2143 cm^{-1} (4.7 μm) and causes absorption at the long

TABLE 8. EXPLOSION PRODUCT VAPORS AND AMBIENT CONCENTRATIONS

	TIGER TNT	TIGER RDX	AMBIENT
CO:	89 ppm	21 ppm	.075 ppm
H_2O:	76	116	2×10^5
CO_2:	125	131	330
CH_4:	25	30	1.6
NH_3:	0.6	0.9	--
HCN:	1.5×10^{-4}	--	--

wavelength side of the 3 - 5 μm window [20]. Figure 8 shows moderate resolution (5 cm^{-1}) transmittance calculated over a 1 kilometer path for ambient and enhanced CO concentrations. The average transmittance in the 4.39 to 5.0 μm region drops from 52% for a midlatitude summer atmosphere with ambient CO concentration to 32% for the same atmosphere with 60 ppm of CO. The rest of the 3 - 5 μm window, the 8 - 12 μm window, and the 1.06 μm and 10.6 μm laser wavelengths are not significantly affected by CO. The drop to near zero transmittance around 2280 cm^{-1} in Figure 8 is a common feature in the 3 - 5 μm region caused by CO_2 and H_2O absorption.

Methane is produced in quantities 20 to 30 times the ambient concentration. The methane infrared active fundamentals are centered at 7.7 μm and 3.3 μm. Figure 9 shows a high resolution plot of absorption coefficients in the 3 - 5 μm window region due to a 30 ppm methane concentration. This plot represents line-by-line calculations using the AFGL line parameter compilation data base [21]. From the figure it is clear that a narrow band instrument operating between 3.0 and 3.5 μm might be strongly affected by methane at 30 ppm, but most of the 3 - 5 μm window is not

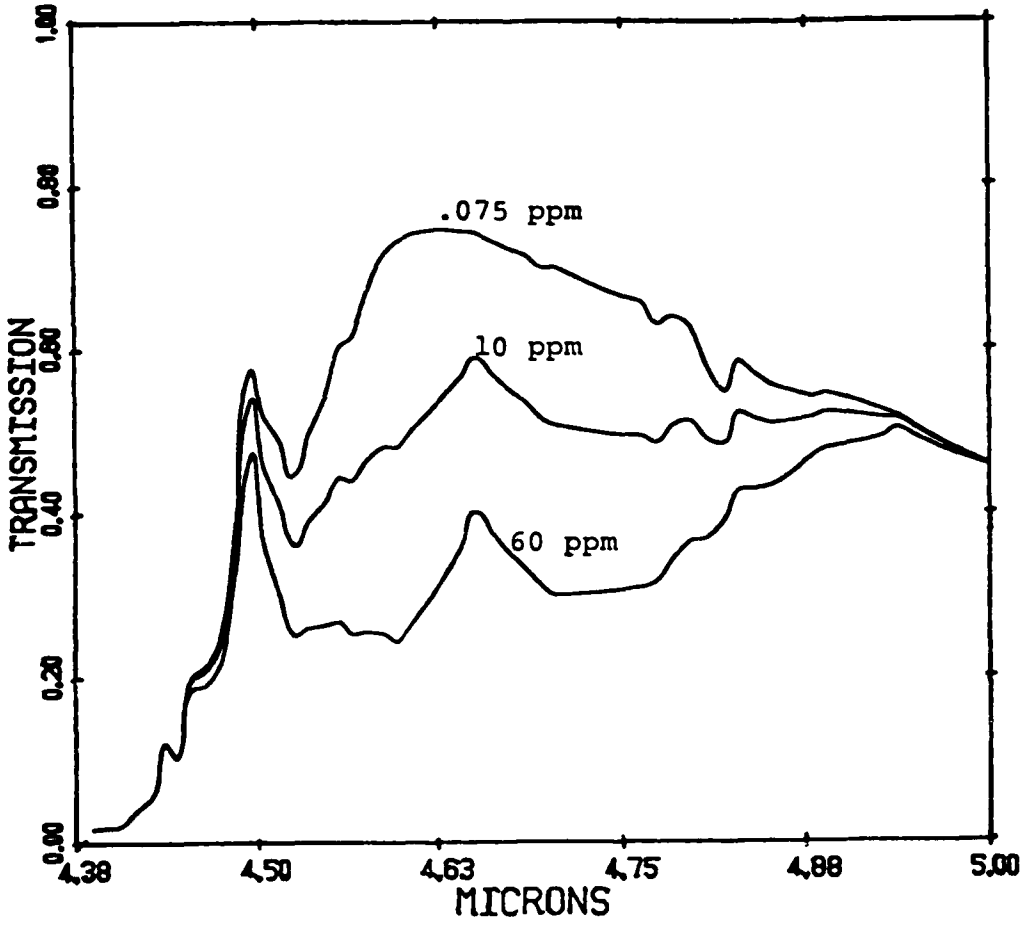

FIGURE 8.TRANSMISSION FROM 4.39 to 5 μm FOR A MIDLATITUDE SUMMER ATMOSPHERE WITH AMBIENT AND ENHANCED CO CONCENTRATIONS

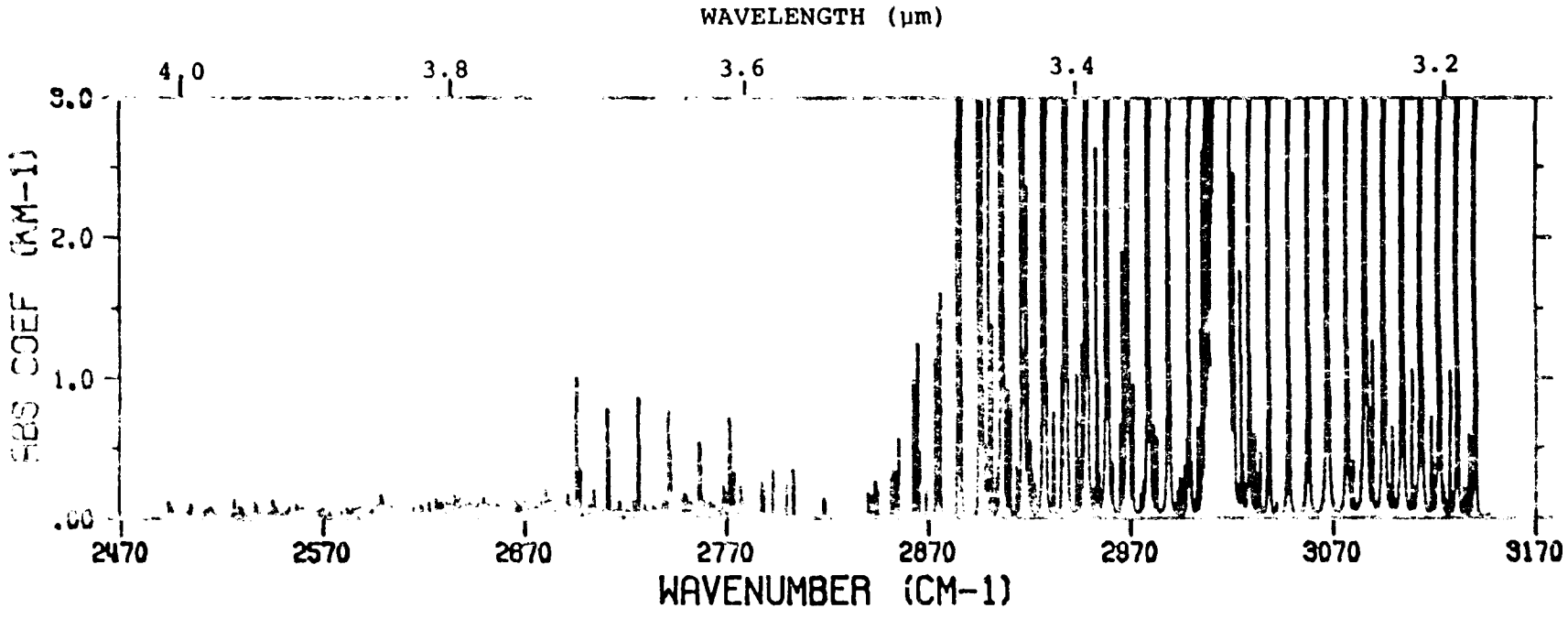

FIGURE 9. ABORPTION FROM 3 TO 4 μm DUE TO 30 ppm OF METHANE

influenced and a broad band instrument would be unaffected. At any rate methane absorption, even at the high methane concentration, is small compared to absorption by ambient H_2O and HDO concentrations in this region.

The 7.7 μm methane band extends into the 8 μm side of the 8 - 12 μm window, as shown in Figure 10. Again, a narrow band instrument in the 8 μm region could experience difficulty, as methane absorption has peaks as high as 4 to 16 km^{-1} at some wavelengths. Broadband absorption in the 8 - 12 μm window is virtually unaffected.

The methane fundamental at 7.7 μm is over 300 cm^{-1} from the 10.6 μm CO_2 laser line P(20), and has negligible influence there.

Ammonia appears in the battlefield atmosphere as a product of high energy explosives. As noted in Section 2.1 the amount of NH_3 predicted by TIGER depends strongly on how equivalent equilibrium is defined, indicating an uncertainty in the final NH_3 concentration.

The strongest feature of the infrared spectrum of NH_3 is the band associated with the ν_2 fundamental at 950 cm^{-1}. Figure 11 is a high resolution plot of absorption coefficients in the 8 to 12 μm region due to 1 ppm of NH_3. The figure plots the results of line-by-line calculations using the AFGL trace gas line parameter data base [22]. Peak absorption is greater than 1 km^{-1} at a number of frequencies. The P(20) laser line of CO_2 lies in a fortunate position between the two NH_3 Q branches. Figure 12 shows absorption coefficients in the 943 to 945 cm^{-1} area due to 10 ppm of NH_3. The individual lines in the figure represent the contributions due to individual NH_3 spectral lines, and the top line represents the sum of these contributions. Since absorption coefficient in km^{-1} scales linearly with concentration,

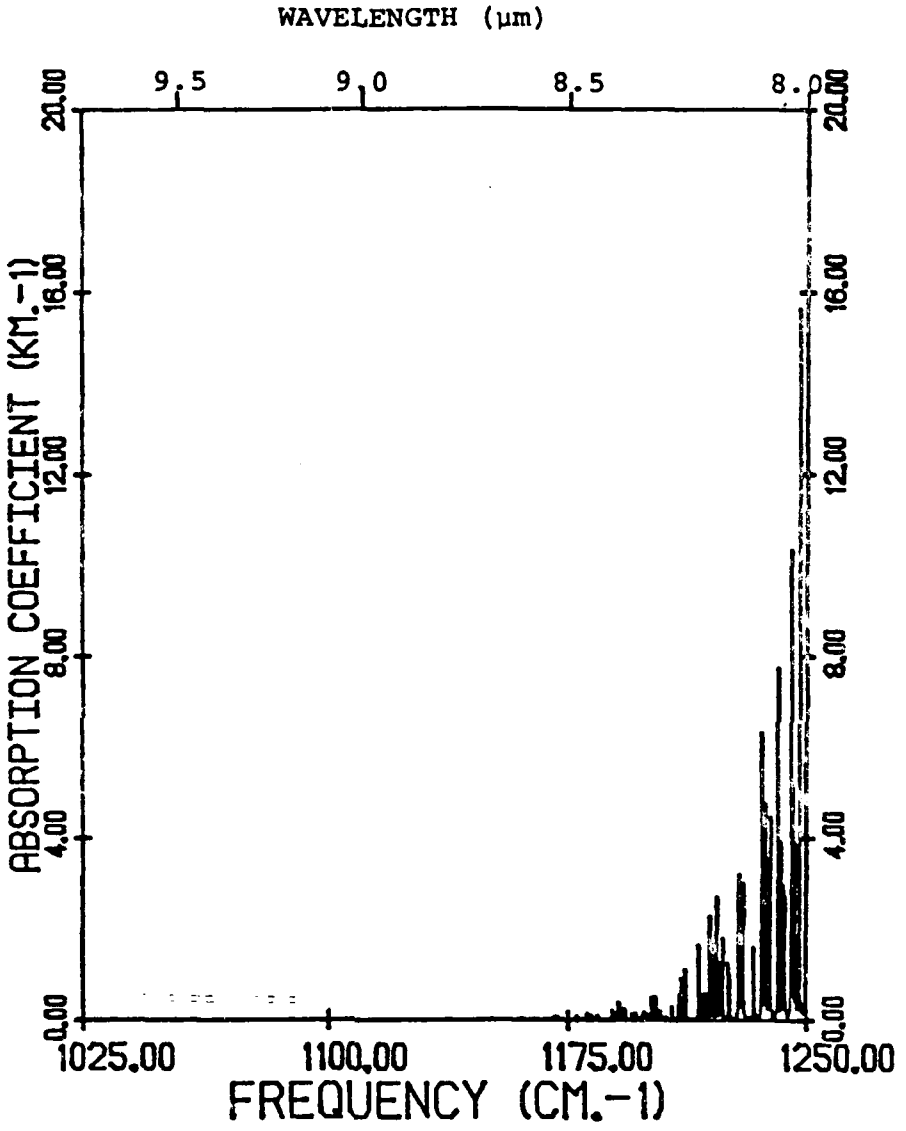

FIGURE 10. ABSORPTION NEAR 8 μm DUE TO 30 ppm of METHANE

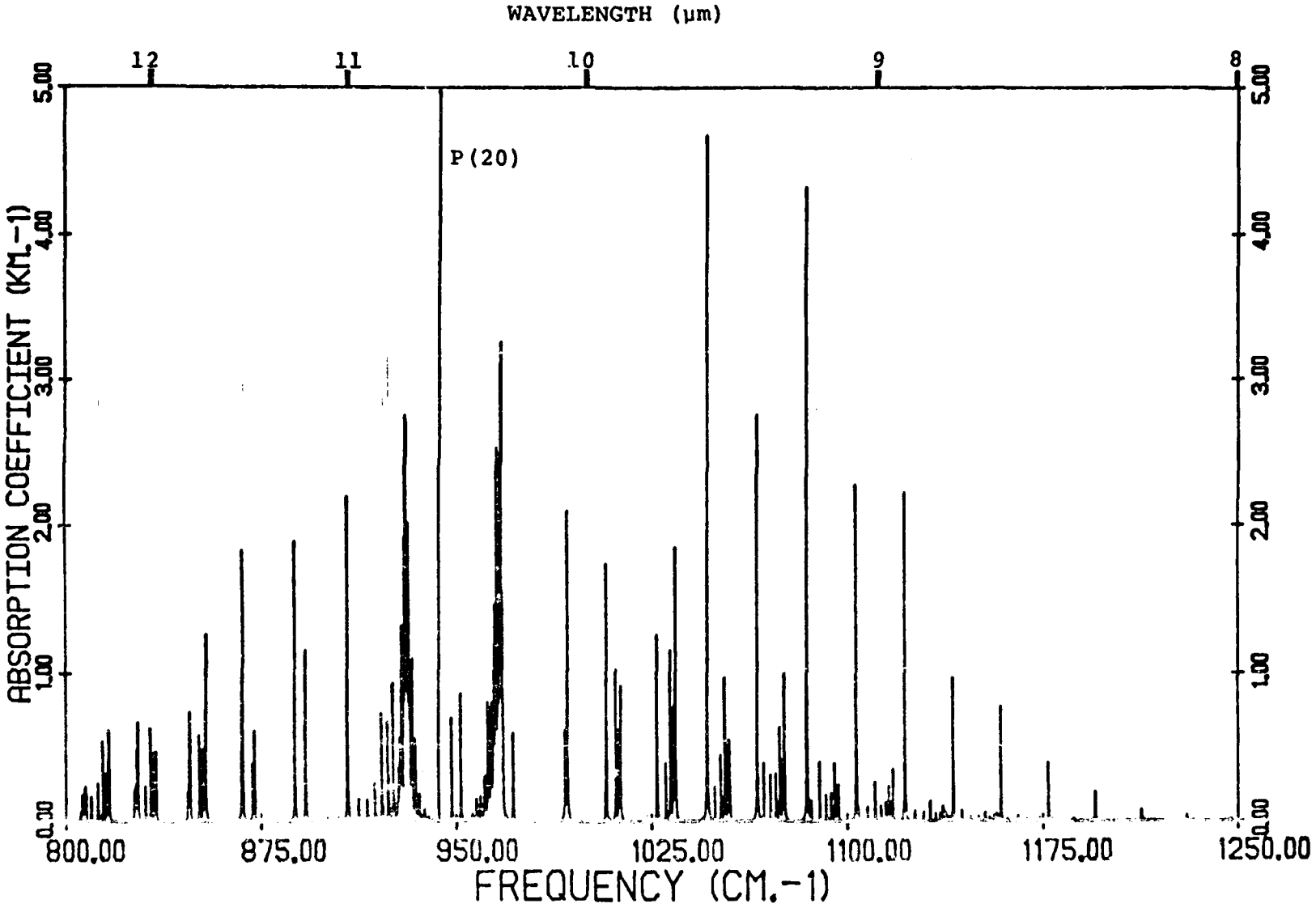

FIGURE 11. ABSORPTION FROM 8 TO 12 μm DUE TO 1 ppm OF AMMONIA

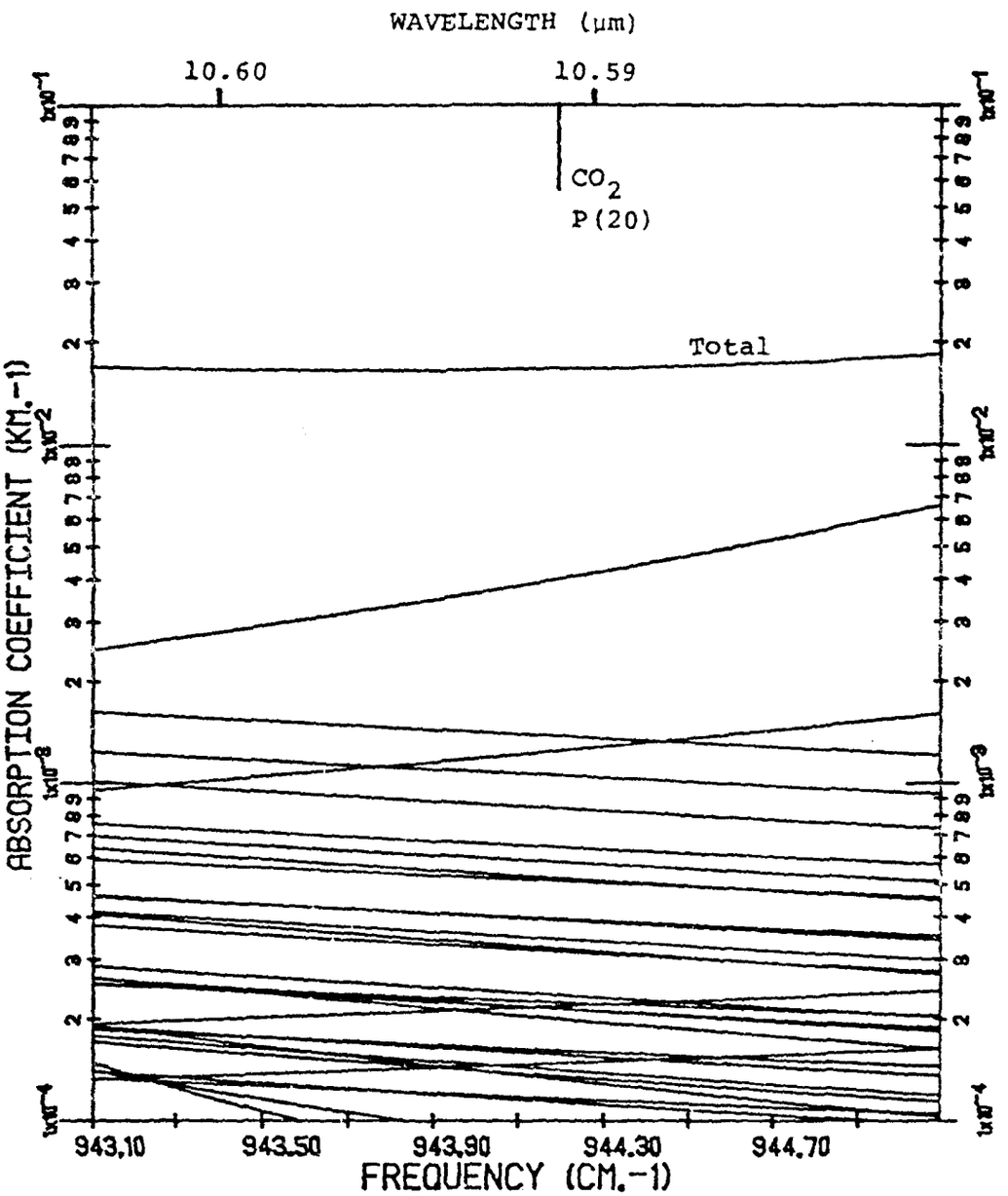

FIGURE 12. ABSORPTION DUE TO 10 ppm OF AMMONIA AT CO_2 LASER LINE P(20)

we can express the absorption at P(20) as km^{-1} per unit concentration; from the figure, this value is 1.8×10^{-3} km^{-1}/ppm. Even at 10 ppm of NH_3 the transmittance at P(20) over a one kilometer path is 98%.

The ν_4 band of NH_3 is centered at around 6 μm and covers the 5 to 8 μm region but causes no absorption in the windows. The ν_1 and ν_3 fundamentals are around 3 μm but these bands and the overtone and combination bands are very much weaker than ν_2.

4.2 OZONE AND NITRIC OXIDE

In Section 2 we discussed the limits of NO and O_3 production via shock chemistry and pointed out that negligible amounts remained after one second or so following detonation. It is instructive, however, to consider the absorption using the initial gas concentration estimates assuming no decrease in the O_3 and NO number densities. We found 8.6 moles O_3 and 1.2 moles NO produced following the blast from 4 kilograms of tetryl. The infrared fundamental of NO lies near 5.3 μm and hence NO poses no problem for CO_2 or DF laser propagation. (But NO lies in the center of the CO laser operating region.) Ozone has vibration fundamentals at 14.1 μm, 9.6 μm, and 5.7 μm. The submillimeter spectrum of ozone is dense and well known [23]. The 9.6 μm band will strongly interfere with CO_2 laser lines in the $(00^{\circ}1) - (02^{\circ}0)$ P manifold centered near 9.6 μm. Again assuming 10^4 four kilogram payloads distributed uniformly over a 1 km^2 area with a 60 meter ceiling yields a concentration of 32 ppm, assuming no dissipation of O_3. The CO_2 laser line most sensitive to ozone appears to be P(40) at 9.404 μm which has an ozone absorption coefficient at 1.51 km^{-1}/ppm [24]. For our hypothetical worst case we then have an absorption

coefficient of 48 km^{-1} or 0.8% transmission of P(40) through 100 meters of 32 ppm uniformly mixed O_3. Were this the case with P(20) of CO_2 at 10.59 μm, a line frequently used in systems applications, then experimental measurements would be called for. However, the O_3 absorption at 10.59 μm is negligible compared to that at 9.6 μm. The possible ozone problem (depending on the accuracy of the blast chemistry, which adequately models smog chemistry) may be worth remembering for

a) submillimeter spectral applications

b) 8 - 12 μm systems using CO_2 laser lines in the 9.6 μm CO_2 band.

4.3 PRODUCTS OF COMBUSTION

In Section 2.3 we discussed several gaseous products of combustion likely to be important for a battlefield scenario. We now apply our diffusion models and estimate important infrared absorption. In the case of burning hay, or foliage in general, we assume one ton of combustible on one square kilometer area burns yielding a smoke cloud of uniformly mixed products with a 50 meter ceiling in the 5×10^{10} liter volume. This results in 1.8×10^{-5} grams of fuel per liter volume. Applying the absorption coefficient of 0.04 $cm^{-1}/g/l$ from Section 2.3, we have 0.73 km^{-1} absorption per ton/km^2 of foliage, or 93% transmission for a one kilometer path in the 10 μm spectral region. Certainly if more than 1 ton/km^2 of foliage burn the absorption in the 8 - 12 μm region increases dramatically. From the curves in the 10 um region in the Southern Research Institute report [11] we see absorption by acetylene C_2H_2 in this region at about 1/4 that of methanol.

Methanol, acetylene, ethylene, etc. are simple hydrocarbons whose presence increases during incomplete combustion. The C-H single bond stretching mode is a common "signature" for these simple hydrocarbons, and the absorption via this mode is usually centered around 3.5 μm, at the high frequency

side of the DF laser region. Previous studies with propane and butane have indicated that DF radiation is attenuated by a few percent per kilometer with propane or butane concentrations of a few parts per million [25]. We expect this to be order of magnitude correct for most of the simple hydrocarbons in the DF region.

A second interesting combustible is rubber. In Table 4 we indicated 0.15 cm^{-1}/gram/liter absorption due to C_2H_4 ethylene, and the same amount due to C_4H_6 butadiene. Both gases are strong absorbers in the 10 μm region. Absorption values for certain CO_2 laser lines have been published in pollution monitoring studies [26]. Normally the CO_2 laser is tuned to that absorption line with maximum overlap with the laser line to provide maximum sensitivity. In the case of ethylene we have several choices, as shown in Table 9. It is clear that P(20) transmission is 24 times better than that at P(14). The rapid change in transmission is due to the C_2H_4Q branch located at 949.2 cm^{-1}.

TABLE 9. CO_2 LASER LINE ABSORPTION BY ETHYLENE

$\nu(cm^{-1})$	CO_2 Line	Absorption
949.5	P(14)	3.6 km^{-1}/ppm
947.9	P(16)	0.46 km^{-1}/ppm
944.2	P(20)	0.15 km^{-1}/ppm

For broadband transmission at 10 μm we can lump the butadiene and ethylene absorption together to give 0.2 cm^{-1}/gram/liter total. Assuming that 30 pounds of rubber burns and the products are confined to the short time volume of 10^6 liters the fuel mass to volume ratio is 1.4×10^{-2}

grams/liter. For a 10 meter optical path we get an optical depth of

$$0.2 \frac{cm^{-1}}{g/l} \times 1.4 \times 10^{-2} \text{ g/l} \times 10^{3} \text{ cm} = 2.8$$

and the transmission is $e^{-2.8}$, or 6% per 30 pounds of rubber burning for a 10 meter path. In computing this estimate we have scaled up from a laboratory spectrum of the products of complete combustion of about one gram of rubber. The uncertainty of such extrapolation is large, and experimental work is needed to provide better data for these kinds of applications. But this estimate shows that this is an area of concern.

For comparison to the broadband estimate we now compute P(20) attenuation. 1.4×10^{-2} grams/liter is equivalent to 8000 ppm by volume if we assume the mass of gaseous products equals the original fuel mass. From Table 9, P(20) absorption is 0.15 km^{-1}/ppm. The optical depth for a 10 meter path is 12, and the transmittance is e^{-12}. The gas is essentially opaque to P(20). This is not meant to be an exact calculation, but rather to indicate an example of the great differences which may arise between broadband absorption coefficients and laser line absorption coefficients.

4.4 VEHICLE EMISSIONS

In Section 2.4 we estimated vehicle emissions for a large diesel engine. We can convert these to atmospheric concentrations under poor atmospheric dispersion conditions by constraining the gases to remain in the 1 km by 1 km area with a 60 meter ceiling described in Section 4.1.

Table 10 lists the results. Table 10 assumes operation of a single tank in the 6×10^{10} liter volume for one hour. It also assumes all the aldehydes appear as formaldehyde, and all the NO generated remains as NO.

TABLE 10. CONCENTRATIONS DUE TO VEHICLES UNDER POOR DISPERSION CONDITIONS

CO_2	1.1 ppm
H_2O	1.0 ppm
CO	40 ppb
NO	50 ppb
CH_2O (formaldehyde)	2 ppb
C_2H_4 (ethylene)	0.25 ppb

By comparison to the ambient concentrations listed in Table 8 we see that CO_2 and H_2O vehicle emissions are completely insignificant. The CO concentration due to vehicle exhaust is of the same order of magnitude as the background concentration.

When NO is introduced into the atmosphere some of it is converted to NO_2. Both NO and NO_2 exist at 1 ppb or less in ambient air, and the concentration of these gases may be sharply increased by vehicular activity. As noted before, NO absorption has no effect at atmospheric windows and common laser frequencies, with the exception of some absorption at the very edge of the 3 - 5 μm window. NO_2 has two infrared bands which overlap window regions. The ν_2 band, centered at 13.3 μm (750 cm^{-1}) extends into the long wavelength edge of the 8 - 12 μm window. Line-by-line calculations using the AFGL trace gas line parameters [22] produce absorption coefficients well below .005 km^{-1} in this region for 50 ppb of NO_2, and this absorption can

safely be neglected. The $\nu_1 + \nu_3$ combination band of NO_2 is centered at 3.4 μm, and absorption coefficients for this band, calculated using line-by-line procedures and the AFGL trace gas line parameters, are shown in Figure 13. These values are for a 50 ppb concentration of NO_2, the predicted amount for one tank per square kilometer under poor dispersion conditions, with all the NO converted to NO_2. A higher density of tanks might generate enough NO_2 to cause 10% absorption over a one kilometer path in the 3.4 μm region under these severe conditions, but NO_2 due to vehicles is not a strong absorber on the battlefield.

Formaldehyde absorption is negligible in the infrared windows. Large concentrations might cause some depletion of millimeter wave radiation, but the amount predicted in Table 10 does not produce significant absorption.

In Section 2.4 we estimated that a tank engine may emit on the order of 0.25 liters per minute of ethylene (C_2H_4), or 7.5 liters per one half hour. Even if confined to our short-term volume of 10^6 liters the 7.5 ppm ethylene yields only 1% absorption at CO_2 laser line P(20) for a 10 meter path. Certainly a large convoy of tanks or troop transports may increase the path over which the ethylene concentration exists, but at first glance we conclude other possible sources of ethylene (foliage combustion) are likely to be more important.

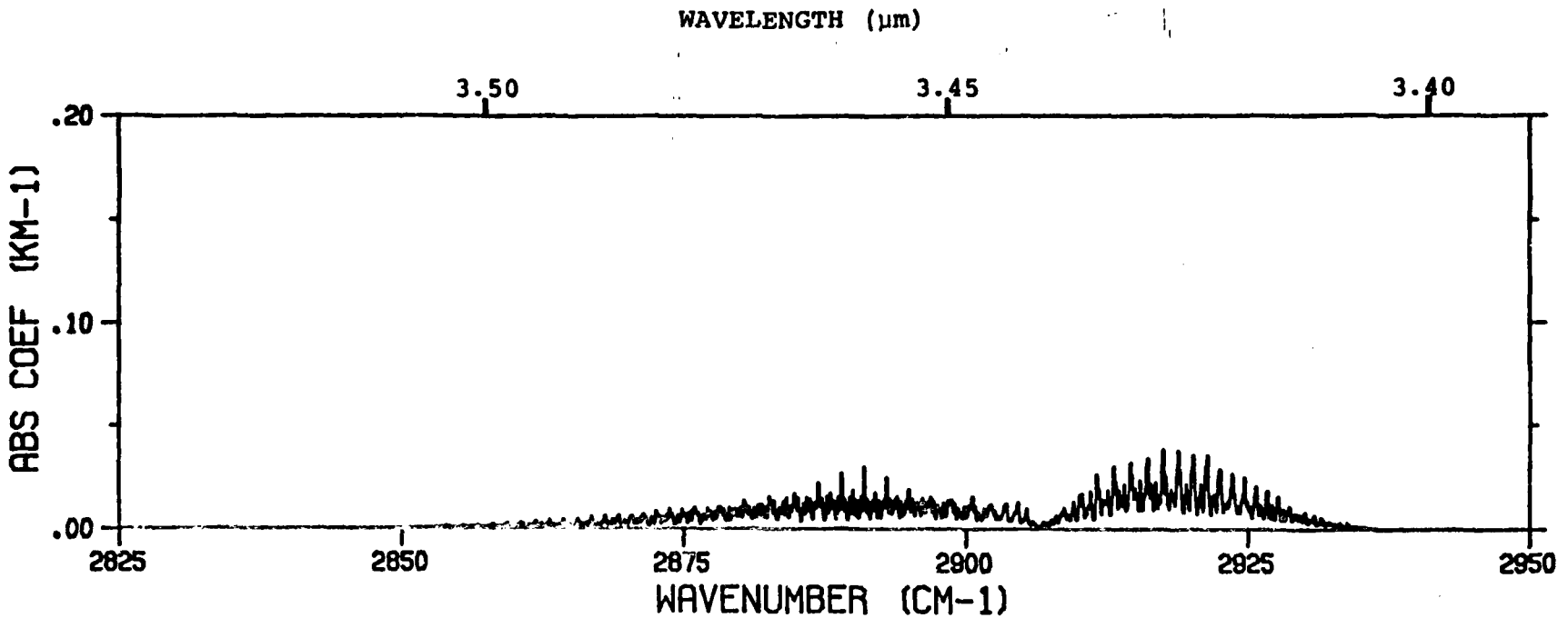

FIGURE 13. ABSORPTION AT 3.4 μm DUE TO 50 ppb OF NO_2

5. CONCLUSIONS AND RECOMMENDATIONS

Concentrations of gases produced by high energy explosives, burning materials, and vehicle emissions were predicted for battlefield situations under fairly restrictive dispersion conditions. The infrared behavior of these gases was used to predict narrow and broadband absorption at 3 - 5 μm, 8 - 12 μm, and 1.06 μm where most IR devices operate.

Heavy absorption was predicted for the products of burning rubber when constrained to a fairly small volume. This allowed only 6% transmission of 8 - 12 μm radiation and completely obliterated the P(20) line of the CO_2 laser over a fairly short path. The situation as described is very localized. A more useful result might have been obtained by using the dispersion model to distribute the products (ethylene and butadiene) and predicting the infrared absorption. The results that were obtained, however, required some extreme extrapolations, and further manipulation did not seem appropriate. We conclude simply that the products of buring rubber may strongly affect broadband 8 - 12 μm and P (20) laser transmission.

Other battlefield gases exhibit absorption in portions of the infrared windows. Although none are expected to exert a strong influence on E-O devices, they are worth noting. High energy explosives produce CO which absorbs at 4.4 to 5.0 μm, CH_4 (3.2 to 3.5 μm and 8.0 to 8.5 μm) and NH_3 (8 to 12 μm). The CO_2 laser line P(20) appears unaffected by NH_3, but it sits precariously between two areas of moderately high NH_3 absorption and its predicted attenuation depends on the accuracy of the NH_3 line positions and strengths. A large

amount of vehicular activity coupled with poor dispersion conditions could produce enough NO_2 to cause very moderate attenuation around 3.4 μm.

There is considerable uncertainty in predicting the effects of burning materials. Combustion products of both natural and man made materials may strongly influence infrared propagation, and experimental work is needed to obtain better parameters for predicting absorption. For example, an analysis of gas concentrations above a burning hay field, along with tests of laser and broadband transmission, would be very useful. Similar experiments might also be run for burning rubber, fuel, and other materials likely to be found in the modern battlefield.

REFERENCES

1. Engineering Design Handbook: Principles of Explosive Behavior, AMCP 706-180, U.S. Dept. of Commerce, AD 900 260, April 1972.

2. J. Alster, U.S. Army ARRADCOM, Dover, New Jersey, private communication.

3. M. Cowperthwaithe and W. Zwisler, Improvement and Modification to Tiger Code, Final Report, SRI Project PYU-1397, January 1973.

4. M. Finger, E. Lee, F.H. Helm, B. Hayes, H. Hornig, R. McGuire, M. Kahara, and M. Guidry, "The Effect of Elemental Composition on the Detonation Behavior of Explosives". Proceedings of the 6th Symposium (International) on Detonation, Coronado, California, 1976, published by the Office of Naval Research, Arlington, Virginia.

5. C.L. Mader, Los Alamos Scientific Laboratory, private communication.

6. D.L. Ornellas, "The Heat and Products of Detonation of HMX, TNT, NM, and FEFO", J. Phys. Chem. 72, 2390-94, 1968.

7. M.A. Cook, The Science of High Explosives, Reinhold Publishing Corp., New York, 1958.

8. J. Alster, Ruby Code Calculations of the Chapman-Jouguet Parameters of Some Novel Explosive Systems, Picatinny Arsenal Technical Report 3416, November 1966.

9. H.M. Sheinfeld, Chemical Properties of Propellants Used in Rockets, Guns, and Small Arms: Foreign, DIA Publication DST 1850W02276 (Confidential).

10. C.W. Wilson, "Air-Blast Generated Battlefield Gases", September 1978, and private communication, Science Applications, Inc., LaJolla, California.

11. W. Barrett, E. Dismukes, J. Powell, Infrared Spectral Studies of Agents and Field Contaminants, Southern Research Institute Annual Report DAAA15-68-C-0154, December 1969 (Confidential).

12. J. Perez, Caterpillar Tractor Co, Peoria, Illinois, private communication.

13. T. Baines, U.S. Environmental Protection Agency, Ann Arbor, Michigan, private communication.

14. D. J. Patterson and N.A. Henein, Emissions from Combustion Engines and Their Control, Ann Arbor Science, 1972.

15. K. J. Springer, J. T. White, and C. J. Domke, Emissions from In-Use Trucks and Buses, SAE Technical Paper 741006, 1974.

16. G. Haltiner and F. Martin, Dynamical and Physical Meteorology, McGraw Hill, New York, 1957.

17. R. K. Dumbauld, Smoke Diffusion Model Computer Program, contract No. DAEA-77-C-0060, U. S. Army Electronics Command, Atmospheric Sciences Laboratory, White Sands Missle Range, New Mexico, 1977.

18. G. A. Briggs, "Some Recent Analyses of Plume Rise Observations", Paper ME-8E, Second International Clean Air Congress, Washington, D.C., Dec. 6-11, 1970.

19. T. J. Welch, The Modern Battlefield - Smokey and Dirty, Aberdeen Proving Ground, July 1977 (Confidential).

20. D. E. Burch and D. Williams, "Total Absorptance of Carbon Monoxide and Methane in the Infrared", Appl. Opt. 1, 587-594, 1962.

21. R. A. McClatchey, W. S. Benedict, S. A. Clough, D. E. Burch, R. F. Calfee, K. Fox, L. S. Rothman and J. S. Garing, AFCRL Atmospheric Absorption Line Parameters Compilation,. AFCRL-TR-73-0096, 1973.

22. L. S. Rothman, S. A. Clough, R. A. McClatchey, L. G. Young, D. E. Snider and A. Goldman, "AFGL Trace Gas Compilation", Appl. Opt. 17, 507, 1978.

23. D. H. Leslie, J. L. Manning, F. G. Smith, C. W. Wilson, Submillimeter Atmospheric Absorption at Normal and Elevated Temperatures, Science Applications Report SAI-78-005-AA, December 1978.

24. R. T. Menzies, "Laser Heterodyne Detection Techniques", in Laser Monitoring of the Atmosphere, G. D. Hinkley ed., Springer-Verlag, New York, 1976.

25. K. O. White and W. R. Watkins, Absorption of DF Laser Radiation by Propane and Butane, Atmospheric Sciences Laboratory, ECOM-5563. June 1975.

26. E. D. Hinkley, R. T. Ku, and P. L. Kelley, "Techniques for Detection of Molecular Pollutants by Absorption of Laser Radiation", in Laser Monitoring of the Atmosphere, E. D. Hinkley ed., Springer-Verlag, New York, 1976.

APPENDIX 1

COMPOUNDS FOR DETONATION PRODUCTS

(TIGER & RUBY LIBRARYS)

AlO	F
Al_2O	F_2O
Al_2O_2	H
Be	HCN
BeBr	HCl
$BeBr_2$	HF
BeF	H_2
BeF_2	H_2O
BrF	He
BrF_3	Mg
Br_2	MgO
CFN	MgOH
CF_2	$Mg(OH)_2$
CF_3	N
CF_4	N_2
CHF_3	Na_2
CH_2F_2	NF_3
CH_3F	NH_2
CH_4	NH_3
CO	NO
COF2	NO_2
CO_2	N_2O
C_2H_2	O
C_2H_6	OH
C_3H_6	O_2
C_3H_8	
CaO	
CaOH	
$Ca(OH)_2$	
Cl	
Cl_2	

APPENDIX 2
REACTIONS IN THE PHOTOCHEMICAL MODEL

Reaction Mechanism

1. $h\nu + NO_2 \rightarrow NO + O$
1a. $O + O_2 + M \rightarrow O_3 + M$
2. $NO + O_3 \rightarrow NO_2 + O_2$
3. $O + HC \rightarrow (b_1)\ RO_2$
4. $OH + HC \rightarrow (b_2)\ RO_2$
5. $O_3 + HC \rightarrow (b_3)\ RO_2$
6. $RO_2 + NO \rightarrow NO_2 + (y)\ OH$
7. $RO_2 + NO_2 \rightarrow PAN$
8. $OH + NO \rightarrow HONO$
9. $OH + NO_2 \rightarrow HNO_3$
10. $h\nu + HONO \rightarrow OH + NO$
11. $NO + NO_2 \xrightarrow{H_2O} 2\ HONO$
12. $NO_2 + O_3 \rightarrow NO_3 + O_2$
13. $NO_3 + NO_2 \rightarrow N_2O_5$
14. $N_2O_5 \rightarrow NO_3 + NO_2$
15. $N_2O_5 + H_2O \rightarrow 2HNO_3$
16. $NO_2 + PARTICULATES \rightarrow PRODUCTS$


DAT
FILM
6